# Noise-controlled oscillations and their bifurcations in coupled phase oscillators

M. A. Zaks,[1] A. B. Neiman,[2,3] S. Feistel,[1] and L. Schimansky-Geier[1,2]
[1]*Institute of Physics, Humboldt-University of Berlin, Newtonstrasse 15, 12489 Berlin, Germany*
[2]*Center for Neurodynamics, University of Missouri at St. Louis, St. Louis, Missouri 63121, USA*
[3]*Department of Physics and Astronomy, Ohio University, Athens, Ohio 45701, USA*
(Received 7 April 2003; published 23 December 2003)

We derive in Gaussian approximation dynamical equations for the first two cumulants of the mean field fluctuations in a system of globally coupled stochastic phase oscillators. In these equations the intensity of noise serves as an explicit control parameter. Its variation generates transitions between three dynamical regimes: (i) stationary, (ii) rotatory and (iii) locally oscillatory (breathing). The latter regime has previously not been reported in studies of globally coupled noisy phase oscillators. Our detailed bifurcation analysis is supported by numerical simulations of an ensemble of coupled stochastic phase oscillators. Similar regimes are also found in simulations of globally coupled stochastic FitzHugh-Nagumo elements.

DOI: 10.1103/PhysRevE.68.066206 PACS number(s): 05.45.Xt, 05.40.−a

## I. INTRODUCTION

Ensembles of nonlinear oscillators are abundant in nature [1]. These are in biology, just to mention a few examples, populations of epithelial sensory cells [2], neurons [3,4], heart cells [5–7] or, on the macroscopic level, swarms of flashing fireflies [8,9] and oscillating populations of species in ecosystems [10]. Outside the living nature, ensembles of oscillators are encountered in different areas of chemistry [11,12] and physics [13–19].

This great variety of systems shares the common tendency to synchronize their oscillatory constituents. This synchronization is caused by the interaction between the elements in the ensemble. It results in the emergence of one or of several collective modes and manifests itself in the adjustment of phases of the individual oscillators [20,21]. Thereby, synchronization serves as a fundamental mechanism of self-organization and structure formation in systems of coupled oscillators [13,22,23].

The dynamics of a single oscillatory element can be cast into a simple form by restricting the description to its phase dynamics along a limit cycle [11]:

$$\dot{\varphi} = \Omega + f(\varphi). \tag{1}$$

Therein $\Omega$ is the natural frequency of the oscillator and the $2\pi$-periodic function $f(\varphi)$ describes the inhomogeneity of the temporal evolution along the limit cycle. In the generic first approximation this function can be modeled by $f(\varphi) \sim a \sin\varphi$ with $a$ being the nonlinearity parameter.

In case of coupled oscillators the equations of individual units have to be complemented by additional terms responsible for their interaction. For most relevant interactions these terms depend on the difference of the individual phases only. These equations can be written as [24–28]

$$\frac{d}{dt}\varphi_i = \Omega - a \sin\varphi_i + \sum_j W_{i,j}(\varphi_j - \varphi_i), \tag{2}$$

where $W_{i,j}(\varphi)$ are $2\pi$-periodic functions. Below we will restrict ourselves to global coupling and investigate the simplest case with $W(\varphi) \sim N^{-1}\sin\varphi$ and $N$ is the number of units in the ensemble.

The generic system (2) has been successfully applied to studies of synchronization and pattern formation in a lot of different situations [11,28]. In particular, if $\Omega > a$ it describes waves, synchronizations and global oscillations of coupled self-sustained oscillators. Contrary, in case $\Omega < a$ the model yields pulse and spiral propagation as well as more complicated structures in coupled excitable units [11]. Studies on mutual synchronization with local and global coupling were extended to the case of nonidentical oscillators, whose natural frequencies ($\Omega \to \Omega_i$) are distributed over some interval [5,24,29–35]. A rich variety of different locally and globally locked, running, pinned and oscillatory-dead states has been reported [36–41]. For random dichotomic perturbations of $\Omega_i(t)$, bistability and oscillatory behavior of globally coupled phase oscillators were found [15,42].

Below we concentrate on noise effects in collective dynamics of globally coupled oscillators (2). In particular, we address the question whether an additive white noise acting independently on every unit in the ensemble can lead to qualitative (or bifurcational) changes in the global response of the system.

The nontrivial role of noise in coupled phase oscillators was underlined in several studies. For example, extremely rich behavior is enforced by multiplicative noise as noise-induced first and second order phase transitions and clustering [43–45]. Spontaneous symmetry breaking entailing a ratchet-like transport mechanism with negative resistance and a hysteretic behavior are subjects of [46–49]. Globally connected ratchets were described in [50].

Here we reconsider the simplest case where statistically independent noise sources with constant intensity are added to Eqs. (2). In Sec. II we derive dynamical equations for the first two cumulants (the mean and the variance) of the ensemble phase

$$\phi(t) = \frac{1}{N}\sum_i^N \varphi_i(t), \tag{3}$$

 

within Gaussian approximation. In similar previous attempts restricted to weak noise a transition to noise-induced oscillations in coupled excitable units was reported [51]. In contrast, our approach remains valid for strong noise as well. We perform a detailed bifurcation analysis (Sec. III) and identify a novel regime of localized or breathing oscillations.

Further on, we support the dynamical analysis of the deterministic cumulant equations by numerical simulations of stochastic phase equations as well as of globally coupled noisy FitzHugh-Nagumo systems (Sec. IV). We show that the increase of noise results in changes of the behavior which are in accordance with the general picture found for the cumulant equations.

## II. THE MODEL AND CUMULANT EQUATIONS

We start with a set of $N$ globally coupled identical nonlinear oscillators which are subject to white noise. The state of each oscillator is characterized by its instantaneous phase $\varphi_i$. We choose one of the most studied examples—the ''active rotators''—introduced in [26]:

$$\dot{\varphi}_i = 1 - a\sin\varphi_i + \frac{W}{N}\sum_{j=1}^{N}\sin(\varphi_j - \varphi_i) + \xi_i(t), \qquad (4)$$

with $i=1,\ldots,N$. Here, the parameter $a$ characterizes the inhomogeneity of the phase rotation. When for an isolated oscillator $a$ is increased across the value 1 a saddle-node bifurcation occurs and the oscillatory regime is replaced by a steady state. The intensity of coupling between the oscillators is measured by the parameter $W$. Finally, the stochastic terms $\xi_i(t)$ correspond to thermal fluctuations modeled by Gaussian white noise with $\langle \xi_i(t_1)\xi_j(t_2)\rangle = 2T\delta_{i,j}\delta(t_1-t_2)$.

Formally, it is possible to choose a ''corotating'' reference frame by introducing a set of variables $\psi_i(t)\equiv\varphi_i(t)-t$, $i=1,\ldots,N$. Then $1-a\sin\varphi_i$ is replaced by $-a\sin\varphi_i$. Equations of this kind have been recently treated in [42]. However, in certain situations the laboratory reference frame is preferable, and below we provide the description of behavior in Eq. (4) from the point of view of the quiescent observer.

Quantitatively, the coherence in an ensemble of oscillators can be measured by complex averaged characteristics

$$\rho_k \equiv \frac{1}{N}\sum_{j=1}^{N} e^{ik\varphi_j} = c_k + is_k, \quad k=1,2,\ldots,\infty, \qquad (5)$$

with $c_k \equiv N^{-1}\Sigma_{j=1}^{N}\cos k\varphi_j$, $s_k \equiv N^{-1}\Sigma_{j=1}^{N}\sin k\varphi_j$ defined in the limit $N\to\infty$. In the completely disordered state all these characteristics vanish identically. On the contrary, in a synchronized state they possess nonzero values. Therefore, it is natural to treat the variables $\rho_k$ as a set of complex order parameters. Among those, of course, the variables $c_1$ and $s_1$ are of special significance.

The dynamics of the collective variables $\rho_k$ obeys the infinite chain of coupled complex-valued equations [27],

$$\dot{\rho}_k = \rho_k(ik - k^2T) - \frac{ak}{2}(\rho_{k+1}-\rho_{k-1}) + \frac{Wk}{2}(\rho_1\rho_{k-1} - \rho_1^*\rho_{k+1}), \qquad (6)$$

complemented by the ''boundary condition'' $\rho_0=1$. In terms of real $c_k$ and $s_k$ this reads as

$$\dot{c}_k = -Tk^2c_k - ks_k - \frac{ak}{2}(c_{k+1}-c_{k-1}) + \frac{Wk}{2}(c_1(c_{k-1} - c_{k+1}) - s_1(s_{k-1}+s_{k+1})), \qquad (7)$$

$$\dot{s}_k = -Tk^2s_k + kc_k - \frac{ak}{2}(s_{k+1}-s_{k-1}) + \frac{Wk}{2}(c_1(s_{k-1} - s_{k+1}) + s_1(c_{k-1}+c_{k+1})),$$

with $c_0=1$, $s_0=0$.

To study possible regimes in such infinite sets of equations, usually a truncation is performed: variables $\rho_k$ with values of $k$ beyond certain $k_0$ are neglected. The description of bifurcations was performed with $k_0=20$ in [27]. Notably, in spite of the formal possibility of a very complicated dynamics in a high-dimensional phase space, the attractors of Eq. (7) are rather simple. Our numerical experiments with $k_0$ up to 100 failed to reveal attracting states other than equilibria or periodic solutions. At nonzero values of noise intensity $T$ the variables $c_k$ and $s_k$ are rapidly decaying with the increase of $k$, thereby justifying a truncation. However, for very small $T$ the ensemble of $\varphi_i$ remains highly ordered, therefore the decay of $c_k$ and $s_k$ becomes visible rather lately, and low values of the truncation level $k_0$ in this parameter region may result in the appearance of numerical artifacts: spurious quasiperiodic or even chaotic attractors.

The very fact that the behavior is low-dimensional hints to the possibility of an alternative, much simpler and computationally less expensive model, in which a small number of variables would deliver an adequate description of dynamics. In fact, such approach would be tantamount to a closure of the infinite set of equations (7). This requires a hypothesis on the distribution of the oscillators in the ensemble. Reconstructed from the values of the $\rho_k$ the distribution has a distinct single-hump shape. Therefore, it appears natural to model this distribution by a Gaussian approximation. We assume that the mean field (3) obeys a time-dependent Gaussian distribution with the mean $m(t)$ and the variance $\sigma(t)$, respectively. Then the order parameters become explicit functions of these first two cumulants:

$$s_k = e^{-k^2\sigma^2/2}\sin km, \quad c_k = e^{-k^2\sigma^2/2}\cos km. \qquad (8)$$

As a result, all $c_k$ and $s_k$ can be expressed through $c_1$ and $s_1$: $c_2=c_1^4-s_1^4$, $s_2=2s_1c_1(s_1^2+c_1^2)$, etc. By virtue of this, the infinite-dimensional Eq. (7) is reduced to a system of the 2nd order:

$$\dot{c}_1 = -s_1 - Tc_1 - \frac{a}{2}(c_1^4 - s_1^4 - 1) + \frac{Wc_1}{2}(1-(c_1^2+s_1^2)^2), \qquad (9)$$

$$\dot{s}_1 = c_1 - Ts_1 - as_1c_1(c_1^2+s_1^2) + \frac{Ws_1}{2}(1-(c_1^2+s_1^2)^2).$$

Alternatively, on eliminating all variables $c_k, s_k$, we arrive at a set of purely dynamical equations for the evolution of the cumulants:

$$\dot{m} = 1 - ae^{-\sigma^2/2}\cosh\sigma^2 \sin m, \tag{10}$$

$$\dot{\sigma^2} = 2T - 2(ae^{-\sigma^2/2}\cos m + We^{-\sigma^2})\sinh\sigma^2.$$

Equations (9) and (10) represent two equivalent parameterizations of the same dynamical system, that is the Gaussian ''truncation'' of the infinite Eq. (7). For an observer who watches the whole entity of rotators in the laboratory frame, the description in terms of cumulants appears to be more convenient, since this set of variables yields the measurable characteristics: the position of the instantaneous center of the distribution and its width. The evolution of the ''microscopic'' system (4) is determined by the immediate positions of the individual oscillators on the circle $0 \leqslant \varphi_i < 2\pi$ and does not depend on their histories: the number of rotations completed by each of these oscillators around the circle. Therefore, the ''macroscopic'' variable $m$ is restricted to a circle, and the phase space of Eq. (10) is a cylinder. Mathematically, of course, the description in terms of $m$ and $\sigma^2$ does not differ from the description in terms of $c_1, s_1$, up to an important distinction: for the latter variables the phase space is a plane (with physically meaningful values lying within the unit circle). As we will see below, this topological difference can be crucial for the interpretation of certain events.

A similar approach was pursued in [51] where the distribution of rotators in Eq. (4) was also assumed to be Gaussian, but only the least order terms in $\sigma^2$ were retained. Notably, in the nonstationary regimes of the dynamical system derived in [51], the variable $\sigma^2$ displayed unbounded growth which indicated to the inconsistency of the model. On the contrary, the presence of higher order terms in Eq. (10) ensures a saturation at finite values of $\sigma^2$.

## III. DYNAMICAL REGIMES AND THEIR BIFURCATIONS

In this section, we describe the bifurcations in Eqs. (10) [or, equivalently, in Eqs. (9)].

Since we are unable to write down the time-dependent solutions as explicit functions of time and the parameters $a$, $W$ and $T$, the respective parts of the bifurcation diagrams are obtained with the help of numerical bifurcation techniques. In contrast, derivation of conditions for the bifurcations of time-independent (stationary) solutions can be reduced to an algebraic problem. This reduction can be done in the following way. On calculating the resultant of the right-hand side (RHS) of Eqs. (9) with respect to either of the variables $s_1$ or $c_1$, we obtain a polynomial equation of the 21st degree for the remaining variable, where the coefficients are explicit functions of $(a,W,T)$. In the 3-dimensional parameter space, all changes in the number of real roots of the latter polynomial occur on a 2-dimensional discriminant surface. The algebraic expression for the discriminant surface in terms of $(a,W,T)$ is far too long and cumbersome to be quoted explicitly; below we merely present the results based on the analysis of this expression. [The same expression is obtained from Eqs. (10) after turning their transcedental RHS into polynomial functions with the help of the substitutions $x \equiv \tan(m/2)$ and $y \equiv e^{-\sigma^2}$.] Since changes in the number of real roots correspond in the phase space to a birth and death of stationary solutions, the knowledge of the location of the discriminant surface characterizes completely the saddle-node bifurcations. Finally, stability of stationary solutions is expressed in terms of the coefficients of the Jacobian matrix; e.g., the Hopf bifurcation requires a vanishing trace of the Jacobian.

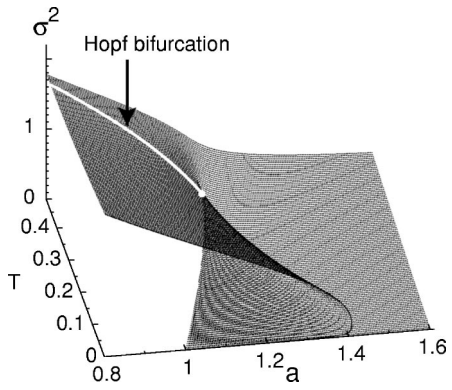


FIG. 1. Steady solutions of cumulant equations (10) at $W=1$. Solid gray line: Hopf bifurcation. Filled gray circle: Takens-Bogdanov bifurcation. Here and below all plotted quantities and parameters are dimensionless.

For the analysis of the time-dependent (periodic, homoclinic) solutions we used a standard 4th order Runge-Kutta integrator. Periodic states were identified as fixed points of the Poincaré mapping on the appropriate curve on the phase plane. Homoclinic bifurcations (existence of trajectories, asymptotical to the saddle point at $t \to \pm\infty$) were identified as ''border'' parameter values at which the numerically reconstructed unstable manifold of the saddle switched between two different attractors.

An analysis of Eqs. (10) shows that in the physically relevant domain of the parameter space, they possess from 1 to 3 steady solutions. The typical situation is represented in Fig. 1. We see that the surface of steady solutions forms two folds which meet in a cusp point. The steady states on the lower leaf of this surface are stable; the ones on the intermediate leaf are always unstable (they correspond to the saddle points). Finally, the states on the upper leaf are unstable for low values of $T$ and stable ''beyond'' the solid line which denotes the Hopf bifurcation.

Complete bifurcation diagrams are presented in Fig. 2. For the description of the bifurcation scenarios it is convenient to consider the following route in the parameter space: fix the values of $T$ and $W$, and proceed by gradually decreasing $a$. High values of $a$ correspond to the domain in which the steady state (fixed point) is unique and globally attracting. If the intensity of noise $T$ is sufficiently high, variation of $a$ does not destabilize this state. However, for low and

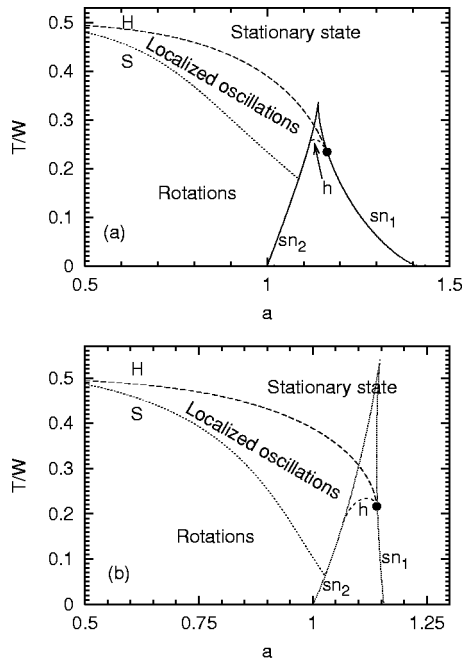


FIG. 2. Bifurcation diagrams of Eq. (10) at $W=1$ (a) and $W=0.25$ (b). $sn_{1,2}$: saddle-node bifurcations; *H*: Hopf bifurcation; *h*: homoclinic bifurcation; *S*: change of type of oscillatory state; filled circle: Takens-Bogdanov point.

moderate values of $T$ the decrease of $a$ leads through a sequence of bifurcations. There are two saddle-node bifurcations: one of them (the right fold in Fig. 1, the line $sn_1$ in Fig. 2) creates two additional steady states: a saddle point and a node, whereas the other one (the left fold, respectively the line $sn_2$) destroys the saddle and the original steady state. For lower values of $a$ the system has an attracting limit cycle. On both curves $sn_1$ and $sn_2$ one of the eigenvalues of the linearization of the flow near the steady state vanishes. On the right branch $sn_1$ of the saddle-node bifurcation, there is a point where the second eigenvalue vanishes as well. This point (the codimension-2 Takens-Bogdanov bifurcation) is an origin of two further bifurcation lines: the Hopf bifurcation and the homoclinic bifurcation. The line *H* of the Hopf bifurcation extends into the domain of lower *a*; for small *a* it tends to $T=W/2$. Above *H*, the steady state is stable, and below this line the stable limit cycle exists.

The curve *h* of the homoclinic bifurcation marks the existence of an orbit which is homoclinic to the saddle point; by definition, this requires the presence of a saddle point, therefore this curve exists only in the ''wedge'' between two lines $sn_{1,2}$ of saddle-node bifurcations. Details of the inner structure of this wedge are presented in Fig. 3. The part of the wedge above the curve of homoclinic bifurcation *h* corresponds to a hysteretic dynamics: in the parameter region between the curves *h*, *H* and $sn_2$ the stable steady state coexists with the attracting limit cycle, whereas in the ''triangle'' delineated by the Hopf bifurcation curve *H* and two saddle-node bifurcations $sn_{1,2}$ two stable steady states are present.

As mentioned above, on the parameter plane the right end point of the curve *h* of the homoclinic bifurcation is the

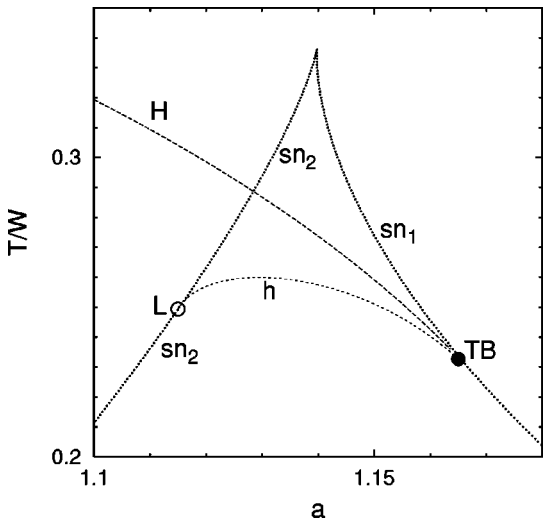


FIG. 3. Enlarged segment of the bifurcation diagram of Eq. (10) at $W=1$. $sn_{1,2}$: saddle-node bifurcations; *H*: Hopf bifurcation; *h*: homoclinic bifurcation; circles: bifurcation points of codimension 2.

Takens-Bogdanov point, denoted as TB in Fig. 3. The left end point of *h* (denoted by *L*) lies on the saddle-node curve $sn_2$. Here, another codimension-2 event takes place: the unstable manifold of the saddle-node point returns back to this fixed point along the ''nonleading'' direction [52]. The segment of $sn_2$ which lies below the point *L*, corresponds to the so-called ''Andronov bifurcation:'' the structurally unstable saddle-node point possesses a homoclinic loop; when *a* is decreased, the fixed point disappears, the loop is destroyed and leaves in the phase space the limit cycle. On this segment of $sn_2$, the saddle-node and homoclinicity are present together; beyond the codimension-2 point *L* they detach, and two separate curves exist: one (the upper segment of $sn_2$) for the saddle-node bifurcation, the other one (the curve *h*) for the homoclinic bifurcation.

Just below the curve *H* of the Hopf bifurcation, the newborn periodic orbit has a small amplitude. When, under fixed *a*, the value of *T* is decreased, this amplitude gradually grows. On reaching the further bifurcation curve, denoted by *S* in Fig. 2, the topology of this periodic orbit in the phase space of *m* and $\sigma^2$ changes: out of a closed trajectory which can be continuously contracted into a point, it becomes a closed curve wrapped around the cylinder. From the point of view of the observer in the laboratory frame, this marks an important qualitative transition: in the dynamics of nonstationary distribution (time-dependent density of rotators) the ''breathing'' oscillations of the center back and forth are replaced by full-circle rotations. In the phase space, this process is mediated by a ''non-physical'' repelling phase trajectory which leads to the infinite point ($m=\pi$, $\sigma^2=\infty$): the periodic orbit ''touches'' this trajectory and changes its topology. This can be viewed as a kind of a global bifurcation: homoclinics to the fixed point which lies at infinity. The increase and subsequent decrease of the amplitude of oscillations in $\sigma^2$ happens rapidly, in a rather narrow parameter interval; several stages of this process are depicted in Fig. 4.

However, strictly speaking this transition is not a true bifurcation but a peculiar projection effect, an imitation of a

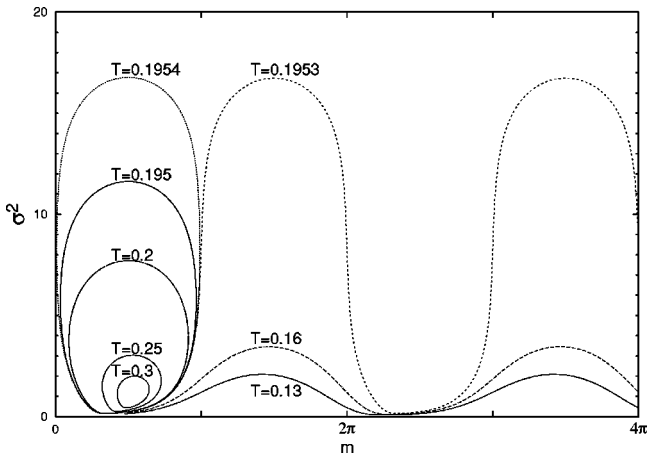


FIG. 4. Transition from oscillations to rotations. Phase portraits of Eq. (10) for $A=1.06$, $W=1$ and various values of $T$. The ''bifurcation'' value is $T_S=0.19535209\ldots$ .

bifurcation: from the point of view of the phase portraits on the plane spanned by variables $c_1$, $s_1$ there are no qualitative changes. The decrease of $T$ leads to the growth of the size of the closed curve corresponding to the limit cycle. At a certain value of $T$ this curve passes through the origin $c_1=s_1=0$. Accordingly, in the course of temporal evolution the distribution of rotators becomes for a short moment perfectly flat; this corresponds to unbounded variance. It is exactly this event which in terms of cumulants $m$ and $\sigma^2$ looks like an excursion to infinity and denotes the transition from localized oscillations to rotations. On the phase plane $c_1$, $s_1$ both states are described by a closed curve; if this curve encircles the origin, the distribution is rotating; if the origin lies outside the curve, the center of the distribution is merely oscillating back and forth.

Since this switching of the periodic orbit is only an ''imitated'' homoclinics, the temporal period of this orbit does not diverge, in contrast to the usual picture of a homoclinic bifurcation. Within the cumulant description, this can be explained by the noncompact character of the event: since the saddle point lies at infinity, both the approach to this point along its stable manifold and the subsequent departure along the unstable manifold occur at infinite speed. Accordingly, the slowdown near the saddle, typical for conventional homoclinic bifurcations, is absent, and the duration of motion along trajectory remains finite.

Of course, near the homoclinic bifurcations which involve the finite-amplitude saddle point, the period of oscillations diverges; on approaching from the left the lower segment of the curve $sn_2$ (Fig. 3) this divergence follows the law of inverse square root, whereas just above the curve $h$ the divergence is logarithmic.

In the setup with fixed parameters $a$ and $W$ and a controllable level of noise, the bifurcations are encountered in different order. If $a$ is chosen to the left of the curve $sn_2$ low noise intensities (i.e., the small values of $T$) correspond to the rotating distribution of oscillators; as $T$ gets larger (on crossing the curve $S$) rotations are replaced by oscillations around a steady state. Further growth of $T$ leads to the decrease of the amplitude of these oscillations; at high values

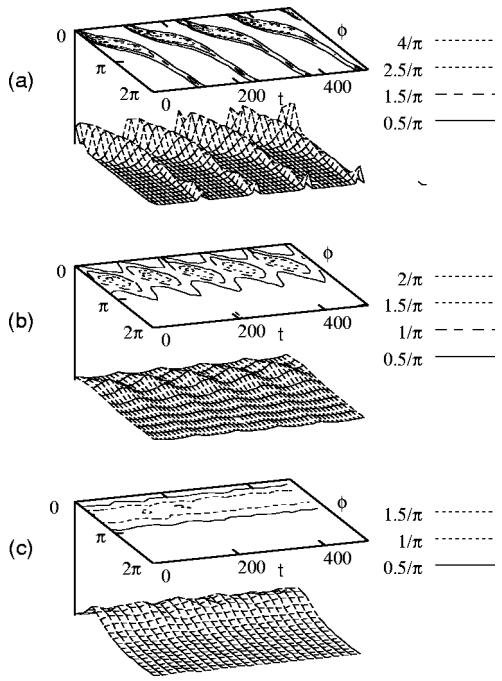


FIG. 5. Distribution of oscillators at $a=0.9$; $W=1$ from direct numerical simulation of $N=10^4$ oscillators governed by Eqs. (4): evolution of instantaneous profiles and isolines of local density $\rho$. (a) Running phase at $T=0.1$; (b) local oscillations at $T=0.25$; (c) steady distribution at $T=0.3$.

of $T$ the steady state (corresponding to the time-independent distribution of mean field) gets stabilized. If the value of $a$ slightly exceeds 1, the sequence of states starts with the time-independent distribution which remains stable within a certain interval of noise intensities. On crossing the curve $sn_2$, this steady state disappears, and the onset of oscillatory regime takes place, with the phase either running around the circle (for lower values of $a$) or oscillating back and forth (for moderate values of $a$). Finally, on the curve $H$ of the Hopf bifurcation, the amplitude of oscillations shrinks and the other steady solution acquires stability. In this way, the intensity of external noise controls whether the mean field of an ensemble of oscillators settles down to a stationary distribution or prefers the distribution which is periodic in time.

Variation of the coupling strength $W$ appears to produce merely the quantitative changes in the bifurcation diagram. With the decrease of $W$ the bifurcation values of $T$ are getting smaller [Fig. 2(b)]; the wedge between the curves of the saddle-node bifurcation becomes sharper: in the deterministic limit $T\to 0$ the line $sn_2$, irrespectively of $W$, begins at $(a=1,T=0)$ whereas the starting point of $sn_1$ for $W\to 0$ tends to $(a=3^{3/4}/2=1.13975\ldots,T=0)$.

To check the above conjectures, we performed direct numerical integrations of Eq. (4) with a set of $N=10^4$ oscillators. Qualitatively, the results correspond to the predictions of the above analysis: for low intensities of noise the relatively sharped peaked distribution rotates around the circle [Fig. 5(a)], for intermediate intensities the oscillations with small amplitude have been observed [Fig. 5(b)] and for high values of $T$ the system settles onto the steady broad distribution [Fig. 5(c)]. Of course, the steadiness of the distribution

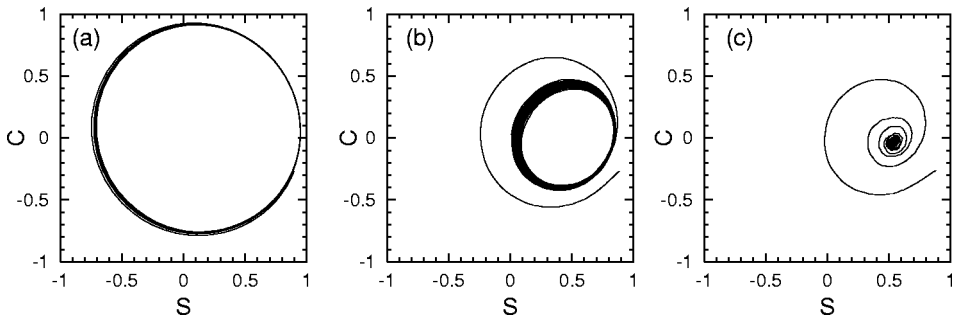


FIG. 6. Phase portraits (with transients) for the order parameter in numerically simulated Eqs. (4) at $a=0.9$; $W=1$. (a) Running phase at $T=0.1$; (b) local oscillations at $T=0.22$; (c) steady distribution at $T=0.3$.

does not imply time independence for individual oscillators; also in the rotating state the angular velocities of the oscillators typically exceed the rate with which the entire distribution rotates around the cylinder. Quantitatively, the threshold values for the transitions between those states turned out to be lower than the values predicted by the bifurcation analysis of Eqs. (10); this can be seen, e.g., by comparison of parameters employed for Fig. 5 with the bifurcation diagram of Fig. 2(a).

Phase portraits for the components $c_1$ and $s_1$ of the complex order parameter are presented in Fig. 6. Noisy limit cycles characterize both the rotating and the locally oscillating distributions; in the former case, the diameter of the cycle is noticeably larger, and the origin lies inside it; in the latter case the origin on the phase plane remains outside the limit cycle. In the case of the stable time-independent distribution, the trajectory spirals to the attracting fixed point.

## IV. ENSEMBLE OF COUPLED FITZHUGH-NAGUMO SYSTEMS

Another illustration of transitions between different dynamical regimes of a mean field is provided by a set of globally coupled FitzHugh-Nagumo elements:

$$\epsilon\dot{x}_i = x_i - \frac{x_i^3}{3} - y_i + \gamma(\overline{x} - x_i),$$

$$\dot{y}_i = x_i + a + \sqrt{2T}\xi_i(t), \tag{11}$$

where $\overline{x} = 1/N\Sigma_{k=1}^{N} x_k(t)$, $N$ is the number of elements in the array, $\gamma$ is the coupling strength, $a$ is parameter of excitability, $\epsilon$ is responsible for the separation of fast and slow time scales, and $T$ is noise intensity.

A single noiseless FitzHugh-Nagumo oscillator possesses an unique stable equilibrium for $a>1$ and a stable limit cycle for $a<1$ which is born through the Andronov-Hopf bifurcation [53].

Equations (11) were simulated numerically for $N=1000$ elements. The coupling strength $\gamma$ was fixed at $\gamma=0.1$. The parameter $a=1.05$ was chosen in the excitable region, so that in the absence of noise each individual element possesses a stable equilibrium. The collective dynamics of the system can be visualized using the mean fields $\langle x(t)\rangle$ and $\langle y(t)\rangle$. An alternative approach is to introduce phases for individual elements and then proceed with the analysis of complex order parameter in the spirit of Eq. (5). The phase of the $i$th element can be estimated as $\varphi_i(t) = \arctan(\dot{x}_i(t)/x_i(t))$ [54]. Then for the ensemble phase defined by Eq. (3) the complex order parameters can be calculated with the help of Eq. (5), like in the ensemble of globally coupled oscillators.

The phase portraits of the system on the plane $\langle x(t)\rangle$, $\langle y(t)\rangle$ are shown in Fig. 7. For weak noise the system possesses a stable equilibrium. With the increase of the

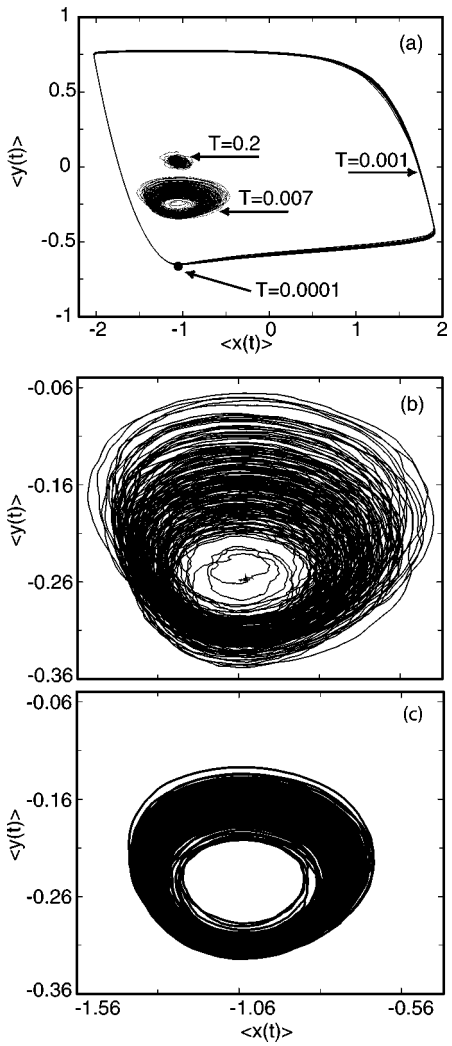


FIG. 7. (a) Phase portraits of the mean field $\langle x(t)\rangle$, $\langle y(t)\rangle$ for $N=10^3$, $a=1.05$, $\gamma=0.1$, $\epsilon=0.01$ and indicated values of noise intensity $T$. Magnified phase portrait at $T=0.007$ for $N=10^3$ (b) and $N=10^4$ (c) elements. Transients are omitted.

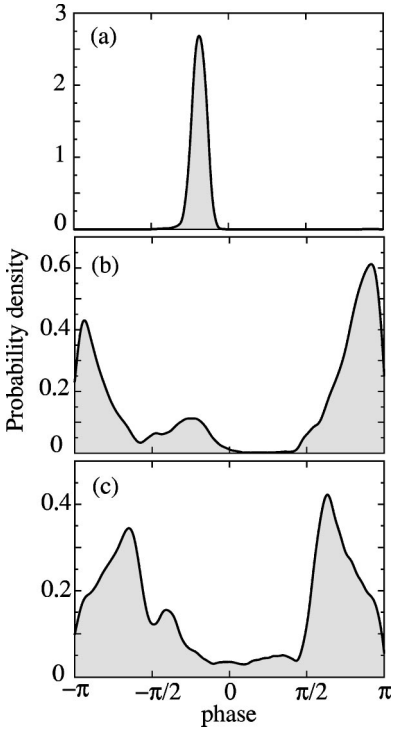


FIG. 8. Instantaneous density of phase distribution in Eq. (11) at (a) $T=0.001$; (b) $T=0.007$; (c) $T=0.2$.

noise intensity a limit cycle is born. The waveform of $\langle x(t)\rangle$ resembles periodic spiking of a single FitzHugh-Nagumo model. As we will see below, this situation corresponds to the running phase solution.

With further increase of $T$ the size of oscillations dramatically shrinks at $T\approx 0.0068$. In this case the waveform $\langle x(t)\rangle$ does not exhibit spikes but rather resembles chaotic motion [Fig. 7(b)]. This case corresponds to local oscillations in the phase model [see, e.g., Fig. 6(b)]. A detailed study of transition to this complex regime is beyond the scope of this paper: in this state the distribution of oscillators is rather far from being single-humped (cf. instantaneous density profiles in Fig. 8) and cannot be properly modeled by the Gaussian approximation.

Here we merely check whether the observed complex motion is robust against a change of the number of elements in the ensemble (see [55] for a discussion of finite size effects on mean field dynamics). In Fig. 7(c) we show the results of simulation of $N=10000$ elements with the same parameters values as in Fig. 7(b) which demonstrate a smeared limit cycle type of attractor. The correlation structure of corresponding processes is qualitatively the same as for the smaller ensemble (see the results of power spectra analysis below). Finally, for large noise intensity the mean field dynamics again collapses to a fixed point, which is apparently different from the equilibrium observed at low values of $T$. Note, that individual elements in both latter cases demonstrate spiking behavior.

Phase portraits for the order parameters $c_1, s_1$ are shown in Fig. 9 for the same parameter values as in the previous plots, and confirm the above conjecture that the increase of noise is accompanied by the transition from the steady state

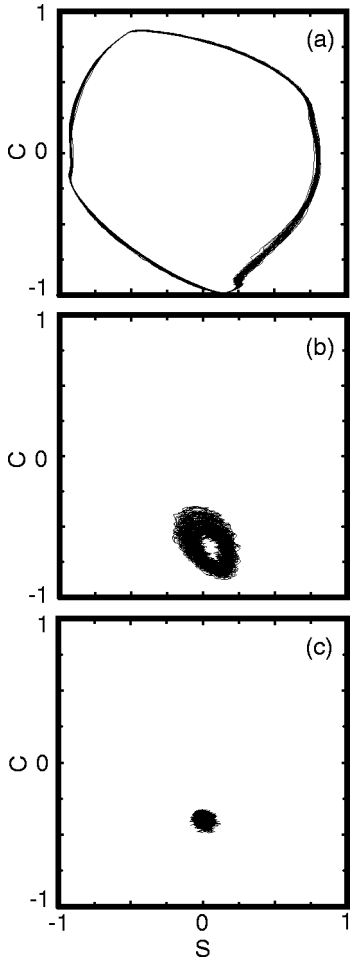


FIG. 9. Phase portraits for the order parameter in Eq. (11). (a) $T=0.001$; (b) $T=0.007$; (c) $T=0.2$. Other parameters are the same as in the previous figure.

through two different kinds of oscillations to the other time-independent distribution.

Finally, we present the power spectra of the observable $\cos\phi$ ($\phi$ the ensemble phase) for three cases of Fig. 9. The evolution of the power spectra is shown in Fig. 10. For small noise intensity, when the mean field possesses a stable fixed point, the power spectrum has an uniform distribution (not shown), resembling that of white noise.

The limit cycle case [Fig. 9(a)] displays well-defined peaks at the main frequency and its harmonics. Transition to the bounded state ($T=0.007$) is characterized by broadened peaks in the power spectrum. Nevertheless, the oscillatory character of this regime is still expressed in the existence of the sharp peak at $\omega=4$ and the broad peak at subharmonics which resembles the power spectrum of a chaotic motion. Note that the qualitative structure of the power spectrum does not change with the increase of the number of elements in the ensemble [solid and dashed lines in Fig. 10(b)]. For large values of noise the oscillations disappear and the power spectrum possesses an uniform structure [Fig. 10(c)].

## V. DISCUSSION

Our analysis has shown that the dynamics of ensembles of coupled noisy oscillators can be efficiently modeled with the

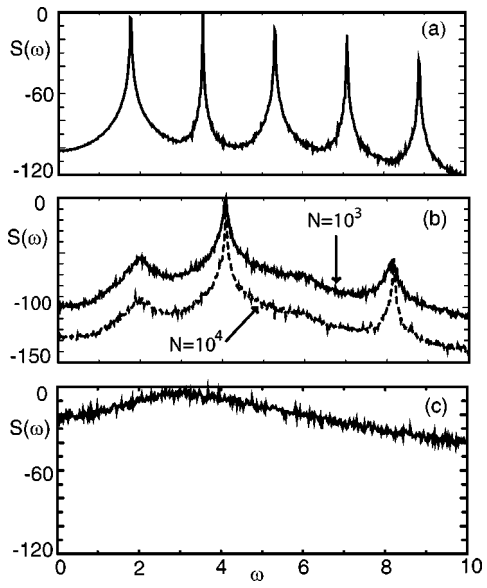


FIG. 10. Power spectra of $\cos\phi$ (ensemble phase) for the ensemble of globally coupled FitzHugh-Nagumo elements (11). (a) $T=0.001$, $N=10^3$. (b) $T=0.007$ for $N=10^3$ (solid line) and $N=10^4$ (dashed line). (c) $T=0.2$. Other parameters are the same as in Fig. 9.

help of deterministic equations which govern the time evolution of the lowest cumulants of the distribution. A natural question in this context is: why does one need this simplified and quantitatively not very precise model when the accurate bifurcation diagram can be evaluated either by direct simulation or by the high-order truncation of the infinite set of coupled equations for the order parameters? The answer, as usually, lies in the transparency and numerical efficiency of the model: in the case of direct stochastic simulations rather high values of the ensemble size $N$ are required in order to minimize finite-size effects, and for the deterministic parameter-order equation the convergence of truncations is usually not especially fast. In addition, the coefficients at linear terms in Eq. (7) grow as $k^2$; this demands to decrease the integration stepsize and, what is worse, makes the high-level truncations of the equation potentially stiff numerically. For the equations with large number of variables, the complete bifurcation analysis cannot be performed; one can only hope that none of the stationary solutions has been missed out by a numerical (Newton-Raphson, etc.) routine. In contrast, Eqs. (10) can be brought to the polynomial form where all steady solutions can be enlisted.

Another important property of the Gaussian model is that it operates in terms of variables which have a transparent meaning. Using the language of distributions, it has been easy to distinguish between the full-scale rotations and the small-amplitude breathing oscillations; noteworthy, the latter state went unnoticed in the previous investigations of dynamics of Eq. (4) [27,51].

Of course, the assumption on the Gaussian distribution, laid in the foundation of the model, is only an approximation. However, the estimation of higher-order moments of the distribution, obtained by direct numerical simulation of Eq. (4) and high-level truncations of Eq. (7) has shown that for the relevant parameter values the distribution is not very far from a Gaussian: the skewness typically does not exceed 0.1 (and is usually much smaller than that), whereas the curtosis is seldom larger than 2.

Further, using closure hypotheses based on the assumption of Gaussian distributions can be promising in more difficult situations, like scattered individual frequencies of oscillators, complicated functional dependencies for inhomogeneities of the phase rotation [$f(\phi)$ in Eq. (1)] and/or for the way in which the individual elements are coupled [$W_{i,j}$ in Eq. (2)]: insights arising from such relatively simple low-dimensional models can give a proper idea of the ensemble dynamics, which otherwise can be obtained only at the cost of long and tedious computations.

## ACKNOWLEDGMENTS

Our research was supported by SFB-555, projects 315/ab of DAAD and INT-0128974 of the NSF. A.B.N. acknowledges support from the National Institutes of Health (Grant No. R01DC004922 to D.F. Russell). We are grateful to R. Kawai, A. Pikovsky, and P. Reimann for stimulating discussions.

[1] S.H. Strogatz, Physica D **143**, 1 (2000).
[2] A.B. Neiman and D.F. Russell, Phys. Rev. Lett. **88**, 138103 (2002).
[3] P. Tass *et al.* Phys. Rev. Lett. **81**, 3291 (1998).
[4] A.K. Engel, P. Fries, and W. Singer, Nature Reviews Neuroscience (London) **2**, 704 (2001).
[5] A.T. Winfree, J. Theor. Biol. **16**, 15 (1967); **28**, 327 (1970).
[6] A. Winfree, *The Geometry of Biological Time* (Springer, New York, 1980).
[7] C. S. Peskin, *Mathematical Aspects of Heart Physiology* (Courant Institute of Math. Sci., New York, 1975).
[8] J. Buck, Q. Rev. Biol. **63**, 265 (1988).
[9] S.H. Strogatz and I. Stewart, Sci. Am. **269**, 102 (1993).
[10] B. Blasius, A. Huppert, and L. Stone, Nature (London) **399**, 354 (1999).
[11] Y. Kuramoto, *Chemical Oscillations, Waves and Turbulence* (Springer, New York, 1984).
[12] I.Z. Kiss, Y. Zhai, and J.L. Hudson, Science **296**, 1676 (2002).
[13] H. Haken, *Advanced Synergetics* (Springer, Berlin-Heidelberg-New York, 1983).
[14] S.H. Strogatz, C.M. Marcus, R.M. Westervelt, and R.E. Mirollo, Physica D **36**, 23 (1989).
[15] S. Kim and M.Y. Choi, Phys. Rev. B **48**, 322 (1993).
[16] T.D. Clark, Phys. Lett. **27A**, 585 (1968).
[17] K. Wiesenfeld, P. Colet, and S.H. Strogatz, Phys. Rev. Lett. **76**, 404 (1996).
[18] F. Ritort, Phys. Rev. Lett. **80**, 6 (1998).
[19] B.J. Kim, M.S. Choi, P. Minnhagen, G.S. Jeon, H.J. Kim, and

M.Y. Choi, Phys. Rev. B **63**, 104506 (2001).
[20] A. Pikovsky, M. Rosenblum, and J. Kurths, *Synchronization–A Universal Concept in Nonlinear Sciences* (Cambridge University Press, Cambridge, England, 2001).
[21] V. S. Anishchenko *et al.*, *Nonlinear Dynamics of Chaotic and Stochastic Systems* (Springer, Berlin-Heidelberg-New York, 2002).
[22] A. S. Mikhailov, *Foundations of Synergetics* (Springer, Berlin-Heidelberg-New York, 1992).
[23] M.C. Cross and P.C. Hohenberg, Rev. Mod. Phys. **65**, 851 (1993).
[24] Y. Kuramoto, in *International Symposium on Mathematical Problems in Theoretical Physics*, edited by H. Araki, Lecture Notes in Physics, Vol. 39 (Springer, New York, 1975).
[25] Y. Kuramoto and I. Nishikawa, J. Stat. Phys. **49**, 569 (1987).
[26] S. Shinomoto and Y. Kuramoto, Prog. Theor. Phys. **75**, 1105 (1988).
[27] H. Sakaguchi, S. Shinomoto, and Y. Kuramoto, Prog. Theor. Phys. **79**, 600 (1988).
[28] J. D. Murray, *Mathematical Biology* (Springer, Berlin, 1993).
[29] I.I. Bonilla, J.M. Casado, and M. Morillo, J. Stat. Phys. **48**, 571 (1987).
[30] K. Wiesenfeld and P. Hadley, Phys. Rev. Lett. **62**, 1335 (1989).
[31] I.I. Bonilla, J.C. Neu, and R. Spigler, J. Stat. Phys. **67**, 313 (1992).
[32] H. Daido, Phys. Rev. Lett. **73**, 760 (1994).
[33] J.D. Crawford, J. Stat. Phys. **74**, 1047 (1994).
[34] C.J. Perez and F. Ritort, J. Phys. A **30**, 8095 (1997).
[35] T. D Frank, A. Daffertshofer, C.E. Peper, P.J. Beek, and H. Haken, Physica D **144**, 62 (2000).
[36] S.H. Strogatz and R.E. Mirollo, J. Stat. Phys. **63**, 613 (1991).
[37] A. Arenas and C.J. Peréz Vicente, Phys. Rev. E **50**, 949 (1994).
[38] A. S. Pikovsky, in *Stochastic Dynamics*, edited by L. Schimansky-Geier and T. Pöschel, Lecture Notes in Physics, Vol. 484 (Springer, Berlin, 1997).
[39] Z. Zheng, B. Hu, and G. Hu, Phys. Rev. Lett. **81**, 5318 (1998); Phys. Rev. E **62**, 402 (2000).
[40] Z. Liu, Y.C. Lai, and F.C. Hoppensteadt, Phys. Rev. E **63**, 055201 (2000).
[41] J.T. Ariaratnam and S.H. Strogatz, Phys. Rev. Lett. **86**, 4278 (2001).
[42] M. Kostur, J. Luczka, and L. Schimansky-Geier, Phys. Rev. E **65**, 051115 (2002).
[43] P. Reimann, C. Van den Broeck, and R. Kawai, Phys. Rev. E **60**, 6402 (1999).
[44] S.H. Park and S. Kim, Phys. Rev. E **53**, 3425 (1996).
[45] S.H. Park, S. Kim, and C.S. Ryu, Phys. Lett. A **225**, 245 (1997).
[46] P. Reimann, R. Kawai, C. Van den Broeck, and P. Hänggi, Europhys. Lett. **45**, 545 (1999).
[47] J. Buceta, J.M. Parrondo, C. Van den Broeck, and F.J. de la Rubia, Phys. Rev. E **61**, 6287 (2000).
[48] S.E. Mangioni, R.R. Deza, and H.S. Wio, Phys. Rev. E **63**, 041115 (2001).
[49] P. Reimann, Phys. Rep. **361**, 57 (2002).
[50] R. Häussler, R. Bartussek, and P. Hänggi, in *Applied Nonlinear Dynamics and Stochastic Systems Near the Millennium*, edited by J. B. Kadtke and A. Bulsara, AIP Conf. Proc. No. 411 (AIP, New York, 1997), pp. 243–248.
[51] C. Kurrer and K. Schulten, Phys. Rev. E **51**, 6213 (1995).
[52] V.I. Lukyanov, Diff. Eq. **18**, 1049 (1982).
[53] A.S. Pikovsky and J. Kurths, Phys. Rev. Lett. **78**, 775 (1997).
[54] Other definitions of instantaneous phase (for example, through the analytic signal approach) lead to qualitatively equivalent behavior for the ensemble phase (3).
[55] A. Pikovsky and S. Ruffo, Phys. Rev. E **59**, 1633 (1999).